Title

Mechanical Analysis of the Short Model Magnets for the Nb $_{3}$Sn Low-β Quadrupole MQXF

Journal

IEEE Transactions on Applied Superconductivity, 28(3)

ISSN

1051-8223

Authors

Vallone, G

Ambrosio, G

Bajas, H

et al.

Publication Date

2018

DOI

10.1109/tasc.2017.2785388

Peer reviewed

Mechanical Analysis of the Short Model Magnets for the Nb_3Sn Low-β Quadrupole MQXF

G. Vallone, G. Ambrosio, H. Bajas, N. Bourcey, D. W. Cheng, G. Chlachidze, P. Ferracin, P. Grosclaude, M. Guinchard, S. Izquierdo Bermudez, M. Juchno, H. Pan, J.C. Perez, S. Prestemon, T. Strauss

***Abstract*—During the development of MQXF, the new Nb3Sn quadrupole to be used in the LHC inner triplets for the High Luminosity upgrade, three short models were tested: MQXFS1, MQXFS3 and MQXFS5. These models differ in the use of thin or thick laminations for the iron components, in the coil design and in the superconductive strands, RRP or PIT. In the MQXF design, the azimuthal prestress is provided at room temperature by means of the bladder-key technology, and it is further increased during the cooldown by the differential thermal contraction of the various components. Four aluminum rods provide the longitudinal prestress. Both systems allow for a flexible control of the amount of prestress applied. As a consequence, it was possible to test the models exploring different azimuthal and longitudinal prestress conditions, in an attempt to understand their impact on the magnet performances. This paper studies the mechanical behavior of these short models, also providing the strain and stresses measured by means of strain gauges installed on the aluminum shell, on the winding poles and on the rods. Finally, the paper compares the measures with the results from FE models.**

***Index Terms*—High Luminosity LHC, Low-β quadrupole, Nb3Sn magnet, Mechanical Performance, Short Model.**

I. Introduction

As a part of the LHC High Luminosity upgrade, LARP and CERN are jointly developing MQXF, a Nb_3Sn quadrupole that will be installed in the LHC triplet regions with two different magnetic lengths, 4.2 m (MQXFA) and 7.15 m (MQXFB) [1]. The upgrade will bring the luminosity up to 3000 fb^{-1} [2]. Three short models, with a magnetic length of 1.2 m, were produced and tested up to this moment: MQXFS1, MQXFS3 and MQXFS5. Strain gauges were used to monitor the mechanics of the structures.

This paper analyzes the mechanical performance of the short models tested up to now. After a brief description of the MQXF design, magnets structure and test history are discussed. Then, the applied prestress and resulting effects on the magnet mechanical performance are analyzed.

Automatically generated dates of receipt and acceptance will be placed here

This work was supported by the High Luminosity LHC Project at CERN and by the DOE through the U.S. LHC Accelerator Research Program.

G. Vallone, H. Bajas, N. Bourcey, P. Ferracin, P. Grosclaude, M. Guinchard, S. Izquierdo Bermudez and J.C. Perez are with the European Organization for Nuclear Research (CERN), 1211 Geneva, Switzerland (e-mail: giorgio.vallone@cern.ch).

G. Ambrosio, G. Chlachidze and T. Strauss are with the Fermi National Accelerator Laboratory, Batavia, IL 80510 USA.

E. Anderssen, D. W. Cheng, M. Juchno, H. Pan and S. Prestemon are with Lawrence Berkeley National Laboratory, Berkeley, CA 94720 USA.

Colour versions of one or more of the figures in this paper are available online at http://ieeexplore.ieee.org.

Digital Object Identifier: xx

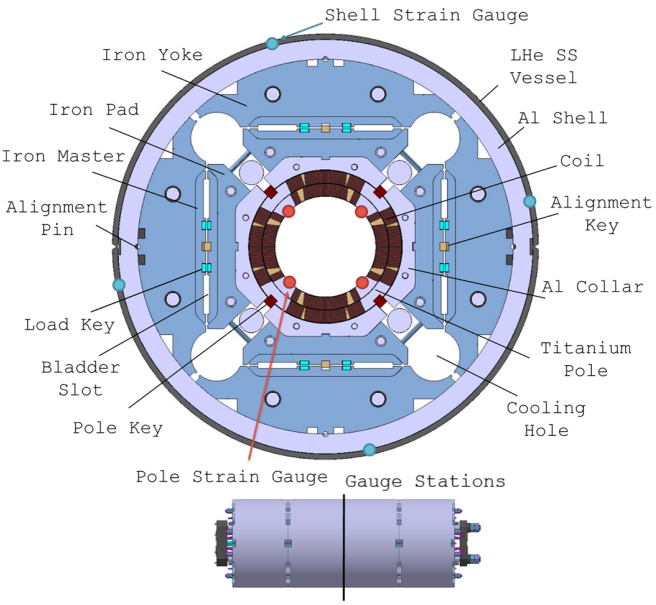

Fig. 1. MQXF cross-section (top), and longitudinal view of the short models (bottom). The LHe SS vessel was not installed during the MQXFS1, MQXFS3 and MQXFS5 experiments. The dots show the strain gauge locations on the shell and the winding poles. The vertical line in the bottom view provides their longitudinal position.

II. MQXF Short Model Magnets

The three short models shared the same cross-section, shown in Fig. 1. This design is the current baseline foreseen for MQXFA and MQXFB magnets. The coils, wound around titanium poles, are held by laminated aluminum collars. An alignment key, inserted in a slot in the pole and in contact with the collar sides, is used to guarantee the alignment of the coil pack to the structure. Around the collars, the magnetic iron is composed of laminated pads and yoke, and bulk masters, used also to accommodate the bladders and the loading keys. Finally, the components are hold by the aluminum shell and the LHe stainless steel vessel. The aluminum shell is longitudinally segmented in order to improve the prestress distribution along the longitudinal axis [3]. The partitioning strategy used is shown in Fig. 1. A detailed description of the magnet design is provided in [1].

The first magnet tested, MQXFS1, used two LARP and two CERN coils, made following the so-called first generation design [4] with RRP conductor. The magnet used 50 mm thick laminations [5] for the iron yoke and pads. The pole alignment key (PK) was made of G10, with the laminations stacked in

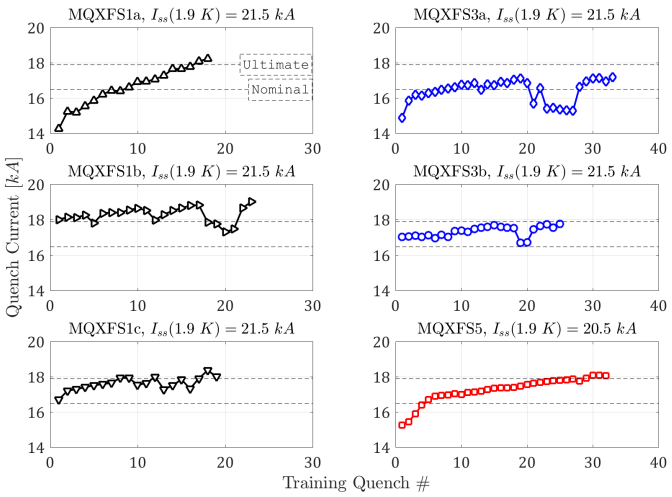

Fig. 2. Short models training curves: the quench current is plotted as a function of the training quench number. Only the quenches at 1.9 K are shown. The title of each subplot reports the short sample current I_{ss} of the magnet.

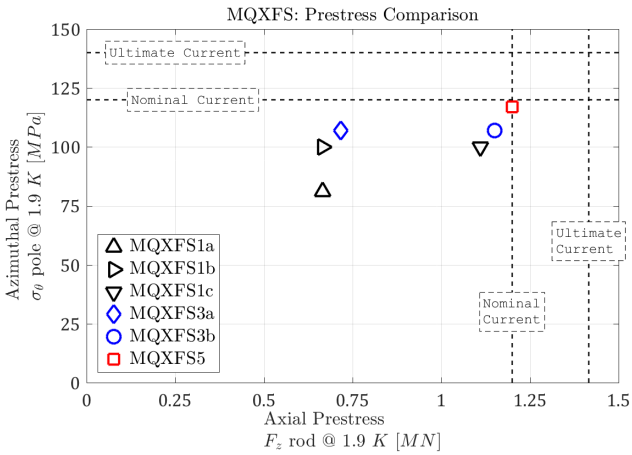

Fig. 3. On the horizontal axis, the total longitudinal force applied by the rods on the coil ends after CD. Vertical dashed lines represent the computed e.m. force at nominal and ultimate current. On the vertical axis, the total azimuthal prestress measured on the winding pole after the CD. Horizontal lines represent the amount of prestress indicatively needed to avoid unloading at nominal and ultimate current.

the azimuthal direction. The magnet was assembled at LBNL and tested at FNAL as MQXFS1a. Fig. 2 shows the MQXFS1 training curve, as well as MQXFS3 and MQXFS5 ones. After reaching ultimate current, equal to 17.89 kA, the magnet was warmed up and the azimuthal prestress was increased. In the following test (MQXFS1b) the magnet kept quenching above the ultimate current. Finally, a longitudinal prestress increase was performed, and the magnet was tested as MQXFS1c. The MQXFS1a mechanics were discussed in [5], [6]. A discussion on MQXFS1 test results can be found in [7], [8].

The MQXFS3 magnet used one LARP and three CERN RRP second generation coils [1]. Thin laminations (5.8 mm) were used for pads and yoke. The PK was made of G10, with the fibers stacked in the radial direction. This new configuration decreases the thermal contraction of the key, and was adopted avoid a possible loss of contact from the collar sides. The magnet was assembled and tested at CERN as MQXFS3a. After failing to reach the ultimate current, an increase in longitudinal prestress was applied. The magnet was re-tested as MQXFS3b, but failed again to reach ultimate current. One coil was identified as the limiting factor, and is currently being substituted before a future test as MQXFS3c.

The MQXFS5 magnet shared the MQXFS3 structure. Four CERN 2-nd generation coils, with PIT conductor, were used. The PK was made of BT-GFRP, with the fibers stacked in the radial direction, as in MQXFS3. This material can withstand high radiation loads: 88% of the flexural strength is kept after 100 MGy irradiation [9]. The magnet managed to reach ultimate current and showed perfect memory after a thermal cycle. Additional details on MQXFS3 and MQXFS5 assembly procedures and shimming plan are provided in [10]. Test results are discussed in [11].

A summary of all the prestresses applied to the MQXF magnets is shown in Fig. 3. The plot shows how, progressing trough the experimental campaign, both the azimuthal and the longitudinal prestress were gradually increased. In fact, the MQXFS1a experiment had demonstrated the magnet capability to reach the ultimate current. However, it required 17 quenches to do so, and showed unloading on the winding pole (see Section III). The increase in prestress tries to improve this behavior. The gradual increase was motivated by an attempt to avoid eventual stress degradation of the conductor [12].

III. Prestress Analysis

The azimuthal and longitudinal prestresses are applied on the coils at room temperature, and then further increased during cooldown by the differential thermal contraction of the components. At room temperature, the azimuthal prestress is provided using the bladder-key technology [13]. The longitudinal room temperature preload is instead provided by means of a piston, putting the aluminum rods in traction, and then holding this deformed state by means of nuts and end-plates.

A. Azimuthal Prestress

The MQXF design allows to control the azimuthal force applied varying the loading key thickness. This force is distributed between the coil and the PK. As a consequence, controlling the contact between the collars and the PK provides additional means to control the total prestress applied to the coil. For example, introducing a gap on the PK sides can reduce the percentage of azimuthal force intercepted by the PK, allowing for two beneficial effects: the required bladder pressure to reach a given pole stress is reduced, as is the amount of force required to the structure. During the experimental campaign, different PK shimming conditions were tested: in MQXFS1, the PK shimming was just enough to obtain contact with the collar sides at the loading start. In MQXFS3, a total interference of 100 μm was applied. In MQXFS5 a total gap of 200 μm was left. The results are shown in Fig. 4, where the Transfer Function (TF), introduced in [5], is used to represent the amount of shell force transfered

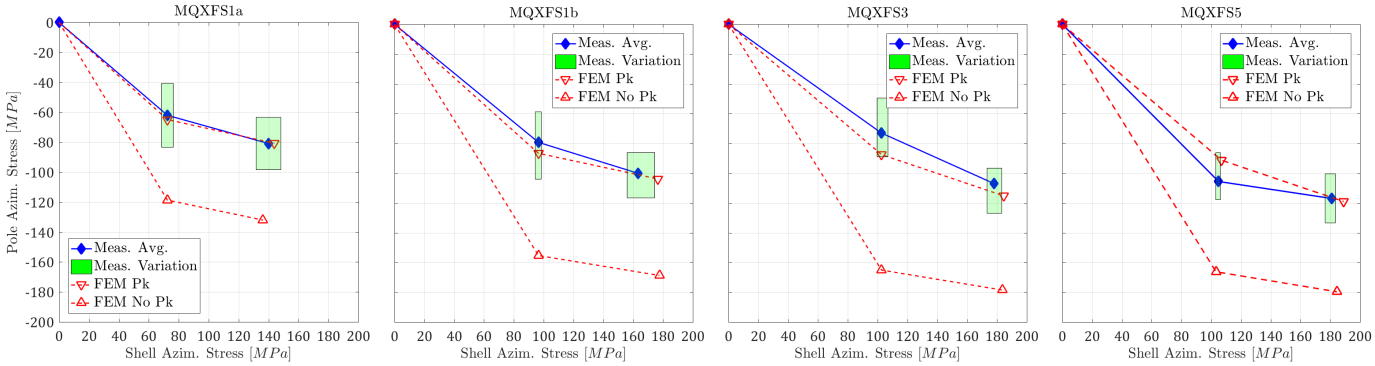

Fig. 4. MQXFS Transfer Functions. The plot show the measured and computed stresses on the winding pole and on shell after the RT loading and the CD. The green rectangles represent the variation of the measurements across the four quadrants. (a): MQXFS1a. (b): MQXFS1b. (c) MQXFS3a (d) MQXFS5.

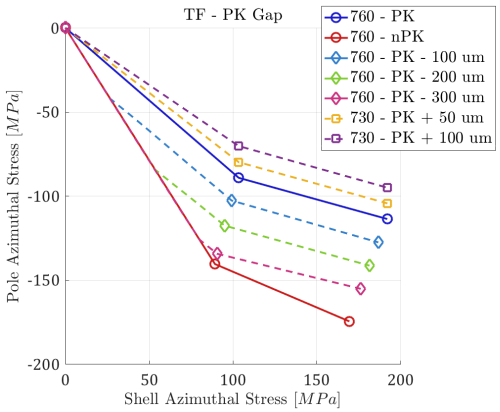

Fig. 5. Computed TF as a function of the applied pole-key interference or gap. The no PK line represents a loading condition where the alignment key does not manage to go in contact with the collar sides. The PK line is obtained when the pole key shimming is just enough to put the key sides in contact with the collars at the start of the loading. The dashed lines represent instead shimming conditions creating gap/interference between the key and the collars.

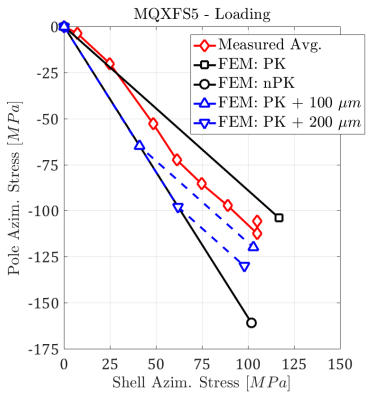

Fig. 6. MQXFS5 loading TF: measured average for growing loading key thickness, compared with the computed values. For this loading, 200 μm of gap were left between the alignment key and the collar sides.

to the coil after room temperature preloading and after cool-down. The continuous lines represent the measured average, and the green rectangles the measured average across the four quadrants. The dashed lines show the expected TF in the 'nominal' conditions, when the PK does not go in contact with the collar sides (no PK line) and when it starts in perfect contact (PK line).

Numerical models can predict the behavior also in intermediate conditions: in Fig. 5, along with the 'nominal' models, dashed lines show the TF when a gap or an interference are applied between the alignment key and the collar sides before loading. For the gap model, the resulting prestress is in-between the 'nominal' conditions. The pole azimuthal stress initially follows the no-PK line, and then moves along the PK line when the PK goes in contact with the collar sides. As the PK is still carrying part of the force, these conditions are still guaranteeing the alignment coil pack-structure. During the MQXFS5 loading, the measurements confirmed this variation of slope, as shown in Fig. 6. The PK went in contact around the expected shell stress. However, a part of the prestress was lost during the first loading steps. This may due to the imperfect contact between the coils and the collars at the start of the loading [14]. The bladder pressure reduction was confirmed: MQXFS3 required a bladder pressure of 490 bar for a final average azimuthal pole stress of 81 MPa; with MQXFS5, only 450 bar were required to reach 112 MPa.

As expected, the TF plots of Fig. 4 show that, during the cool-down, the differential thermal contraction increases both the shell azimuthal stress and the winding pole stress. In MQXFS1a and MQXFS1b, the increase of pole azimuthal stress was equal to 19 MPa. This value can be matched by the numerical models [5]. MQXFS3a/b average pole azimuthal stress at cold was equal to -107 MPa, corresponding to a 34 MPa increase. Finite element models show that this increase with respect to MQXFS1 is due to the new direction of the pole key fibers. MQXFS5 average pole azimuthal stress at cold was equal to -117 MPa. The pole azimuthal stress increase was only 11 MPa. There is no clear understanding of this behavior at the present moment. However, no data on the BT-GFRP elastic properties at cryogenic temperatures was available. An unexpected variation of the properties may contribute to this effect.

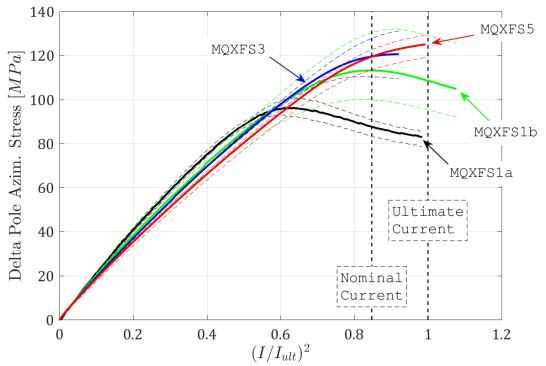

(a)

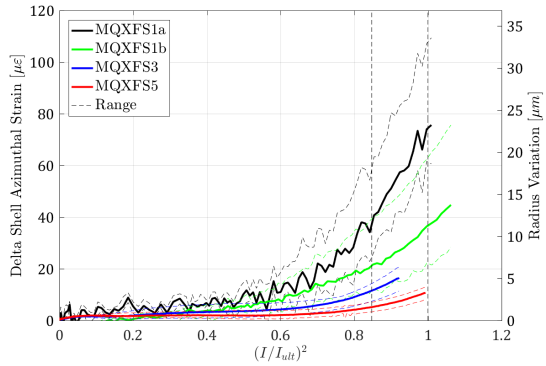

(b)

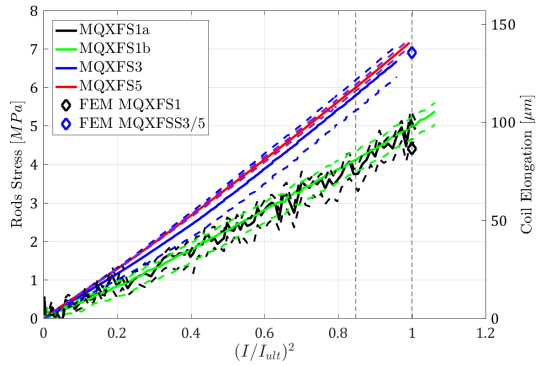

(c)

Fig. 7. Strain gauge measurements during magnet powering. (a) Comparison of measured delta pole azimuthal stress: average (continuous lines) and variation across the quadrants (dashed lines). (b) Delta azimuthal stress on the shell. The auxiliary y-axis on the right shows the radius variation extracted from the strain. (c) Delta stress on the rods, along with the equivalent total coil elongation on the auxiliary y-axis.

B. Longitudinal Prestress

The total longitudinal electromagnetic force at nominal current is equal to 1.2 MN. MQXFS1a, MQXFS1b and MQXFS3a used a rods prestress producing about half of this value of rods longitudinal force at cold. This corresponds to a room temperature rod longitudinal strain of 800 $\mu\varepsilon$. On MQXFS3b and MQXFS5, the longitudinal prestress was increased to 1.12 MN after cool-down, corresponding to a strain of 2500 $\mu\varepsilon$. The measured strain was very uniform across the four quadrants, with a variation of about ± 100 $\mu\varepsilon$. The comparison with numerical results demonstrated that cool-down effect can be predicted with remarkable accuracy, thus giving precise control of the total rods force at cold.

C. Magnet Powering

As the current increases, the electromagnetic forces gradually pull the coil from the winding pole. Fig. 7a shows the evolution of the measured delta azimuthal pole stress during powering. Initially, the stress linearly decreases with the applied forces. The slope is slightly different for each magnet. MQXFS3 and MQXFS5, for example, showed a slightly lower slope than MQXFS1a/b. This effect is not explained for the moment. After a certain level, different for all the magnets, the winding pole stress does not vary linearly anymore. This sudden change is considered an indication of prestress exhaustion and detachment of the coil from the winding pole [15].

The magnet with the lower prestress, MQXFS1a, shows how the curve gradually decreases after reaching its maximum value. Numerical models, including the detachment of the coil from the winding pole, demonstrated that at the maximum the pole is indeed experiencing tension, and that the stress is null at the end of the ramp. As a consequence, a maximum tension of 10 MPa has to be considered when computing the prestress [15]. The total azimuthal prestress in presence of unloading can be then computed as the maximum measured delta stress minus 10 MPa. Experience shows that the prestress computed in this way generally produces the most reliable results. For example, it was essential to evaluate correctly the MQXFS1b TF, shown in Fig. 4b. In fact, the gauge acquisitions during the cool-down showed a very large increase of the pole stresses. In a first moment, the new behavior was interpreted as a detachment of the pole-key from the collar sides. However, often during magnet powering the strain gauges are subject to sudden jumps, introducing an offset in the measurements. To study this effect, MQXFS3 winding pole compensator strains were monitored separately from the pole strain. The experiment showed that also the compensator strain may subject to these jumps during powering. As a consequence, the strain readings after cool-down do not always provide a reliable estimate of azimuthal prestress. The stress increase was in reality very close to the numerical computations, and the PK has to be considered still in contact on both collar sides. Also the estimated MQXFS3 prestress, considering the pole unloading, is about 10 MPa higher than the measurement after cool-down. This is consistent with the computed result. A precise estimate was not possible for MQXFS5, as the curve still did not reach its own maximum. However, the prestress can be roughly extrapolated to be about 117 MPa, about 5 MPa higher than the measurements after cool-down.

Fig. 7b shows the delta azimuthal strain measured on the shell during powering. The signals show very small variations up to a certain current level, and then suddenly start to increase. It was shown in [15] that this slope variation can be explained by the detachment of the coil from the pole, as the one seen in the winding pole strain. In fact, the slope variation appears simultaneously on the shell and on the

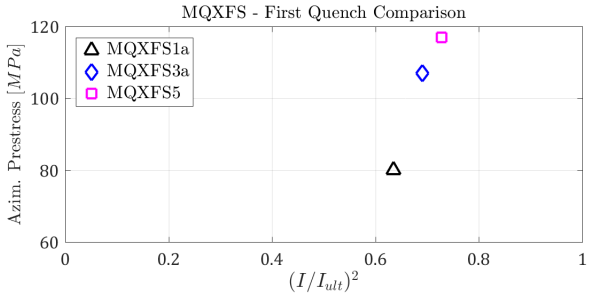

Fig. 8. Azimuthal prestress applied against the first quench current of the MQXFS magnets against. The plot suggests a linear relationship between the two, but will have to be confirmed by future measurements.

winding pole. This also results in a maximum radius variation that is decreasing with lower prestresses. At nominal current, the average radius increase was $12\,\mu$m for MQXFS1a, $5\,\mu$m for MQXFS1b, $3\,\mu$m for MQXFS3 and $2\,\mu$m for MQXFS5.

Measurements on the rods of the three short models are shown in Fig. 7c, along with the equivalent coil elongation. The comparison between MQXFS1a and MQXFS1b suggest that the longitudinal stiffness is not affected by the amount of azimuthal prestress. The comparison between MQXFS3a and MQXFS5 similarly suggest that also the amount of longitudinal prestress does not affect the total elongation. A different longitudinal stiffness is measured on MQXFS1 and MQXFS3/5. The difference may be due to the iron laminations thickness, affecting the longitudinal stiffness of the iron; or to the material used for the radial shimming of the coil pack: G10 in MQXFS1 and Kapton for MQXFS3 and MQXFS5. This could change the friction between coil and collars. In principle, the two effects should be modeled numerically lowering the longitudinal modulus of the yoke or varying the friction between collars and coil. But, as its effect on the rods strain should be similar, it can be reproduced by varying the friction coefficient. Numerical results, shown in Fig. 7c, reproduce closely the measurements for both structures with a modest variation of the friction coefficient: from 0.16 for MQXFS1 to 0.13 for MQXFS3/5.

IV. Prestress Impact on Training

Th azimuthal prestress applied on the virgin magnets and the first quench currents are resumed in Fig. 8. The small amount of data points available does not allow to establish if a relationship does exist between these quantities. However, as the short sample limit decreased [8], [11], the first quench current increased. This may suggest that the quench current could be governed by a mechanical phenomenon, even if it is not possible to clarify its origin. The training curves of these magnets, shown in Fig. 2, also shows that the magnets with higher prestress required less quenches to reach the nominal current. The same does not apply for the ultimate current.

V. Conclusion

The mechanics of the MQXF short models produced up to this moment were analyzed. The paper discussed how the magnet prestress can be controlled intervening both on the loading key thickness and on the amount of shimming applied on the alignment key. The MQXFS5 experiment demonstrated that leaving a gap on the pole key sides can increase the amount of prestress applied, reducing in the meantime the required structure load and bladder pressure. The impact of the cool-down on the pole azimuthal prestress was studied. The experiments showed how the most accurate estimate of the available prestress is given by the pole azimuthal stress during magnet powering. The total azimuthal prestress applied to the magnets ranged from $80\,\mathrm{MPa}$ and $117\,\mathrm{MPa}$. Longitudinal prestress applied was equal to $0.6\,\mathrm{MN}$ for MQXFS1a and MQXFS3a and $1.12\,\mathrm{MN}$ for MQXFS3b and MQXFS5.

The data available suggests that a relationship between the azimuthal prestress and the first quench current may exists. Further experiments are needed to confirm this hypothesis and eventually clarify its nature.

References

[1] P. Ferracin *et al.*, "Development of MQXF: The Nb_3Sn low-β quadrupole for the HiLumi LHC," *IEEE Transactions on Applied Superconductivity*, vol. 26, no. 4, pp. 1–7, 2016.

[2] L. Rossi and O. Brüning, "High Luminosity Large Hadron Collider: a description for the European Strategy Preparatory Group," CERN, Geneva, Swtizerland, CERN-ATS-2012-236, 2012.

[3] M. Juchno *et al.*, "Support structure design of the Nb_3Sn quadrupole for the High Luminosity LHC," *IEEE Transactions on Applied Superconductivity*, vol. 25, no. 3, pp. 1–4, 2015.

[4] E. Todesco *et al.*, "Design studies for the low-β quadrupoles for the LHC luminosity upgrade," *IEEE Transactions on applied superconductivity*, vol. 23, no. 3, 2013, Art. ID 4002405.

[5] G. Vallone *et al.*, "Mechanical performance of short models for MQXF, the Nb_3Sn low-β quadrupole for the Hi-Lumi LHC," *IEEE Transactions on Applied Superconductivity*, pp. 1–5, 2016.

[6] H. Pan *et al.*, "Assembly tests of the first Nb_3Sn low-β quadrupole short model for the Hi-Lumi LHC," *IEEE Transactions on Applied Superconductivity*, vol. 26, no. 4, pp. 1–5, Jun. 2016.

[7] G. Chlachidze *et al.*, "Performance of the first short model 150-mm-aperture Nb_3Sn quadrupole MQXFS for the High-Luminosity LHC upgrade," *IEEE Transactions on Applied Superconductivity*, vol. 27, no. 4, pp. 1–5, Jun. 2017.

[8] S. Stoynev *et al.*, "Summary of test results of MQXFS1 - the first short model 150 mm aperture Nb_3Sn quadrupole for the High-Luminosity LHC upgrade," *IEEE Transactions on Applied Superconductivity*, 2017, Under Review.

[9] A. Idesaki *et al.*, "Development of high radiation-resistant glass fiber reinforced plastics with cyanate-based resin for superconducting magnet systems," *Fusion Engineering and Design*, vol. 112, pp. 418–424, 2016.

[10] S. I. Bermudez *et al.*, "Geometric field errors of short models for MQXF, the Nb_3Sn low-beta quadrupole for the high luminosity LHC," *IEEE Transactions on Applied Superconductivity*, 2017, Under Review.

[11] H. Bajas *et al.*, "Test results of the short models MQXFS3 and MQXFS5 for the HL-LHC upgrade," *IEEE Transactions on Applied Superconductivity*, 2017, Under Review.

[12] H. Felice *et al.*, "Performance of a Nb_3Sn quadrupole under high stress," *IEEE Transactions on Applied Superconductivity*, vol. 21, no. 3, pp. 1849–1853, 2011.

[13] S. Caspi *et al.*, "The use of pressurized bladders for stress control of superconducting magnets," *IEEE Transactions on Applied Superconductivity*, vol. 11, no. 1 II, pp. 2272–2275, 2001.

[14] P. Ferracin *et al.*, "Mechanical performance of the LARP Nb_3Sn quadrupole magnet LQS01," *IEEE Transactions on Applied Superconductivity*, vol. 21, no. 3, pp. 1683–1687, Jun. 2011.

[15] G. Vallone and P. Ferracin, "Modeling coil-pole debonding in Nb_3Sn superconducting magnets for particle accelerators," *IEEE Transactions on Applied Superconductivity*, 2017, Under Review.